nature communications

Article

https://doi.org/10.1038/s41467-025-57750-5

Genomic structural variation in an alpha/beta hydrolase triggers hybrid necrosis in wheat

Received: 3 June 2024

Accepted: 3 March 2025

Published online: 18 March 2025

Check for updates

Yaoqi Si[1,9], Huaizhi Zhang[1,9], Shengwei Ma[2,9], Shusong Zheng[1,9], Jianqing Niu[2,3], Shuiquan Tian[1], Xuejia Cui[1,4], Keyu Zhu[1], Xiaocui Yan[5], Qiao Lu[1], Zhimeng Zhang[1], Tingting Du[1], Ping Lu[1], Yongxing Chen[6], Qiuhong Wu[6], Jingzhong Xie[1], Guanghao Guo[1], Mengjun Gu[7], Huilan Wu[1], Yiwen Li[1], Chengguo Yuan[8], Zaifeng Li[5], Zhiyong Liu[1,3,4] ✉, Lingli Dong[1] ✉, Hong-Qing Ling[1,2,3,4] ✉ & Miaomiao Li[1] ✉

Hybrid necrosis, a century-old mystery in wheat, is caused by complementary genes *Ne1* and *Ne2*. *Ne2*, encoding a nucleotide-binding leucine-rich repeat (NLR) immune receptor, has been cloned, yet *Ne1* remains elusive. Here, we report that *Ne1*, which encodes an alpha/beta hydrolase (ABH) protein generated by structural variation, triggers hybrid necrosis with *Ne2* by activating autoimmune responses. We further verify that not only allelic variation but also copy number variation (CNV) of *Ne1* are pivotal for hybrid necrosis diversity in wheat. *Ne1* likely originates from wild emmer wheat, potentially through duplication and ectopic recombination events. Unlike *Ne2*, which is frequently selected for rust resistance in wheat breeding, the lower prevalence of *Ne1* in modern wheat cultivars is attributed to its association with hybrid necrosis. Altogether, these findings illuminate the co-evolution of the *NLR/ABH* gene pair in plant development and innate immunity, offering potential benefits for wheat breeding.

Hybrid necrosis represents a prevalent phenomenon observed in plant hybrids and is recognized as a common form of genetic incompatibility contributing to gene-flow barriers[1,2]. It arises from epistatic interactions between divergent alleles contributed by different parents in certain hybrids, resulting in autoimmune-like symptoms in the absence of pathogens, including leaf necrosis, crinkling, dwarfism, stunted growth, and reduced fertility[1,3]. Hybrid necrosis has been documented across various species, including *Arabidopsis thaliana*[4], *Capsella*[5], wheat[6], rye[7], lettuce[8], rice[9], and cotton[10]. The genetic basis of hybrid necrosis aligns with the principles of the Bateson-Dobzhansky-Muller (BDM) model, generally involving two-locus interactions[11,12]. The BDM model asserts that a genetic change at locus *A* in one population and a genetic change at locus *B* in another population may be incompatible when residing in the same genome upon the hybridization between individuals of the two populations, which could result in postzygotic incompatibility and lead to infertility or inferiority[13].

Emerging genetic and biochemical evidence indicates that hybrid necrosis is closely linked to plant immune responses. Numerous causal genes associated with hybrid necrosis have been identified, the

[1]Key Laboratory of Seed Innovation, Institute of Genetics and Developmental Biology, Chinese Academy of Sciences, Beijing, China. [2]Yazhouwan National Laboratory, Sanya, Hainan Province, China. [3]Hainan Seed Industry Laboratory, Sanya, Hainan Province, China. [4]College of Advanced Agricultural Sciences, University of Chinese Academy of Sciences, Beijing, China. [5]Hebei Agricultural University, Baoding, Hebei Province, China. [6]Xianghu Laboratory, Hangzhou, Zhejiang, China. [7]Biomedical Research Center for Structural Analysis, Shandong University, Jinan, Shandong, China. [8]Hebei Gaoyi Stock Seed Farm, Gaoyi, Hebei, China. [9]These authors contributed equally: Yaoqi Si, Huaizhi Zhang, Shengwei Ma, Shusong Zheng. ✉e-mail: zyliu@genetics.ac.cn; lldong@genetics.ac.cn; hqling@genetics.ac.cn; mmli@genetics.ac.cn

majority of which encode proteins related to immunity. The *Arabidopsis* hybrid necrosis genes, *Dangerous Mix 1* (*DM1*) and *DM3d*, and the cotton hybrid lethality gene *Le4* are known to encode nucleotide-binding leucine-rich repeat (NLR) immune receptor proteins[4,10]. The *Arabidopsis* DM3 protein, a member of the ABH family, interacts with the NLR protein DM2 is associated with hybrid necrosis[3]. In lettuce, hybrid necrosis is governed by specific isoforms of *Rin4*, which is recognized for its interactions with various resistance (R) genes[8]. Epistatic interactions between *NPR1* and *RPP5* orthologues result in genetic incompatibility within *Capsella* species[5]. Rice *Hwi1* and *Hwi2*, which encode an LRR-RLK immune receptor and a subtilisin-like protease, respectively, activate the autoimmune response in interspecific hybrids[9].

Structural variations, including copy number variations (CNVs) and chromosomal rearrangements, exert substantial influence on the genomic landscape of plants[14]. In particular, CNVs have been recognized as potent drivers of genetic diversity by instigating alterations in gene dosage and expression levels[15]. For example, CNVs contribute to grain size diversity in rice[16] and enhance nematode resistance in soybean[17]. In addition, genomic structural changes and copy number variation at the *Sc* locus confer japonica–indica hybrid male sterility in rice[18].

Hybrid necrosis in wheat has been initially documented by Sax[19]. Hybrid necrosis has been reported in both intraspecific crosses of common wheat[6] and interspecific crosses between tetraploid wheat and *Aegilops tauschii*[20]. Hybrid necrosis impedes the genetic improvement of wheat, acting as a barrier to both the integration of desirable traits from diverse common wheat genotypes and the introgression of genes from related species into commercial cultivars[6]. Hybrid necrosis in common wheat is controlled by the complementary dominant genes *Ne1* and *Ne2*, which are located on chromosome arms 5BL and 2BS, respectively[21]. In 2021, three independent groups successfully cloned and characterized *Ne2*, which encodes an NLR protein[22–24]. *Ne2* is the same gene as wheat leaf rust resistance gene *Lr13* and allelic to wheat stripe rust resistance gene *Yr27*, exhibits pleiotropic effects against rust and hybrid necrosis[23,25]. However, the causal gene for *Ne1* has yet to be determined, despite the development of high-density genetic maps by three separate teams[26–28].

In this study, we report the map-based cloning of *Ne1* using two separate genetic populations. *Ne1* is validated by mutagenesis and transgenic approaches. We also trace the ancestral lineage of *Ne1* and highlight the influence of allelic and copy number variations of *Ne1* on the phenotypic diversity of hybrid necrosis in wheat. Furthermore, we investigate the prevalence of *Ne1* in worldwide tetraploid and hexaploid wheat.

Results

Phenotypic characterization of hybrid necrosis in wheat

Previously, we cloned *Ne2* from wheat line M114 (*Ne1Ne1Ne2Ne2*), which is identical to wheat leaf rust resistance gene *LrZH22*/*Lr13* from Zhoumai 22 (ZM, *ne1ne1Ne2Ne2*)[23] (Supplementary Data 1). M114 showed necrosis symptoms starting at the leaf tips, which spread with plant development, while ZM remained healthy (Fig. 1a and Supplementary Fig. 1a, b). The F_1 hybrids from M114 × ZM displayed necrosis confined to the leaf tips without base involvement at the grain filling stage (Fig. 1a). The 356 $F_{2:3}$ progenies of the M114 × ZM population segregated as 79 homozygous necrotic, 182 segregating, and 95 normal families, conforming to a 1:2:1 single Mendelian locus ratio ($\chi^2_{1:2:1} = 1.617$, $P < 0.05$) (Supplementary Data 2).

We also identified hybrid necrosis in a segregating population derived from wheat accessions Zhengnong 17 (ZN17, *ne1ne1Ne2Ne2*) and Yangbaimai (YBM, *Ne1Ne1ne2ne2*), with *Ne2* cloned from ZN17[22]. To evaluate the necrotic syndrome, we generated a pair of near-isogenic lines, NIL-*ne1* (*ne1ne1Ne2Ne2*) and NIL-*Ne1* (*Ne1Ne1Ne2Ne2*), at the *NE1* locus. Necrosis was characterized by premature leaf death and impaired growth potential (Supplementary Fig. 1c), initially appearing on the tip of basal leaves (Supplementary Fig. 1d). The 3,3′-diaminobenzidine hydrochloride (DAB) staining indicated that excessive localized hydrogen peroxide (H_2O_2) accumulation may trigger leaf lesions (Supplementary Fig. 1e), similar to the hypersensitive response (HR) induced by pathogens.

Map-based cloning of *Ne1*

Bulked segregant RNA-Seq (BSR-Seq) experiments were performed to map *Ne1* on chromosome arm 5BL using M114 × ZM segregating population (Supplementary Fig. 2). We then used 7,659 F_2 individuals from M114 × ZM to narrow down *Ne1* within a 0.07 cM genetic interval flanked by markers *XM14* and *XM6* (Fig. 1b and Supplementary Data 3), corresponding to a 3.61 Mb genomic region according to Chinese Spring (CS) genome sequence IWGSC RefSeq v2.1[29] (Fig. 1c and Supplementary Data 4), overlapping with genetic interval of *Ne1* using ZN17 and YBM population[26] (Fig. 1d). Due to previous report of genomic structural variations at the *NE1* locus[26], we developed specific markers based on the fifteen high-confidence genes in the *Ne1* genomic interval to investigate M114 and ZM. The results show that M114 has a long genomic fragment insertion at the *NE1* locus compared to ZM (Supplementary Fig. 3).

The long insertion fragment specifically encompasses six high-confidence genes, designated as *TraesCS5B03G0561600*-*TraesCS5B03G0564000* according to IWGSC RefSeq v2.1[29] (Fig. 1c and Supplementary Data 4). Notably, *TraesCS5B03G0561800* (*ABH.1*), encodes an alpha/beta hydrolase (ABH) family protein, which is recognized for its roles in plant immunity, such as ABH family proteins EDS1 and PAD4[30,31], as well as *Arabidopsis* hybrid necrosis protein DM3 (At3g61540, ABH family protein) as an interactor of NLR protein DM2[3]. In addition, *TraesCS5B03G0565000* (*ABH.2*), which also encodes an ABH family protein, is located within the *Ne1* genetic interval but not on the long insertion fragment. However, sequence analysis revealed no sequence differences within *ABH.2* between ZN17 and YBM. Therefore, *ABH.1* is considered the likely candidate for *Ne1*.

We then cloned the complete genomic sequences of *ABH.1* from M114 and YBM using specific primers (Supplementary Data 3). *ABH.1* comprises eleven exons (Fig. 1e) and encodes an ABH family protein that contains a hydrolase domain, an AAA ATPase with vWA domain, and a membrane protease YdiL domain (Fig. 1f). Sequence comparison between $ABH.1^{CS}$ and $ABH.1^{M114}$ revealed one T/C SNP at the first intron and another C/G SNP at the sixth exon, resulting in a proline to alanine (P691A) amino acid substitution in the ABH.1 protein (Fig. 1e). Compared to $ABH.1^{CS}$, a 9 bp insertion and a 3 bp deletion (AGCTCAGTT/CAA) was observed at the fifth exon of ABH^{YBM}, resulting in codon insertions/deletions (DN423-424EAQF) (Fig. 1e).

Mutagenesis and transgenic assay validation of the *ABH.1* as *Ne1*

To verify the role of *ABH.1*, seeds of necrotic lines NIL-*Ne1* and M114 were mutagenized with ethyl methanesulfonate (EMS). A total of 4500 and 2360 M_2 families from NIL-*Ne1* and M114, respectively, were screened for non-necrotic leaf phenotype in the field. Finally, 11 and 14 M_3 non-necrotic lines were identified from the NIL-*Ne1* and M114 EMS-mutagenized populations, respectively. The complete genomic sequences of *ABH.1* and *Ne2* were amplified and sequenced from the non-necrotic mutants. Five NIL-*Ne1*-derived non-necrotic mutants (N-m45, N-m61, N-m70, N-m81, and N-m119) and six M114-derived non-necrotic mutants (M114-m1 to M114-m6) displayed a distinct EMS-induced single nucleotide change (G/C to A/T) in *ABH.1* (Fig. 2a, b). Moreover, three NIL-*Ne1*-derived non-necrotic mutants (N-m04, N-m28, and N-m34) and six M114-derived non-necrotic mutants (M114-m7 to M114-m12) exhibited missense mutations in *Ne2*. Two mutants (M114-m13 and M114-m14) harbored nonsense mutations resulting in a premature stop codon in *Ne2* (Fig. 2c, d). The identification of multiple independent EMS non-necrotic mutants from two necrotic

https://doi.org/10.1038/s41467-025-57750-5

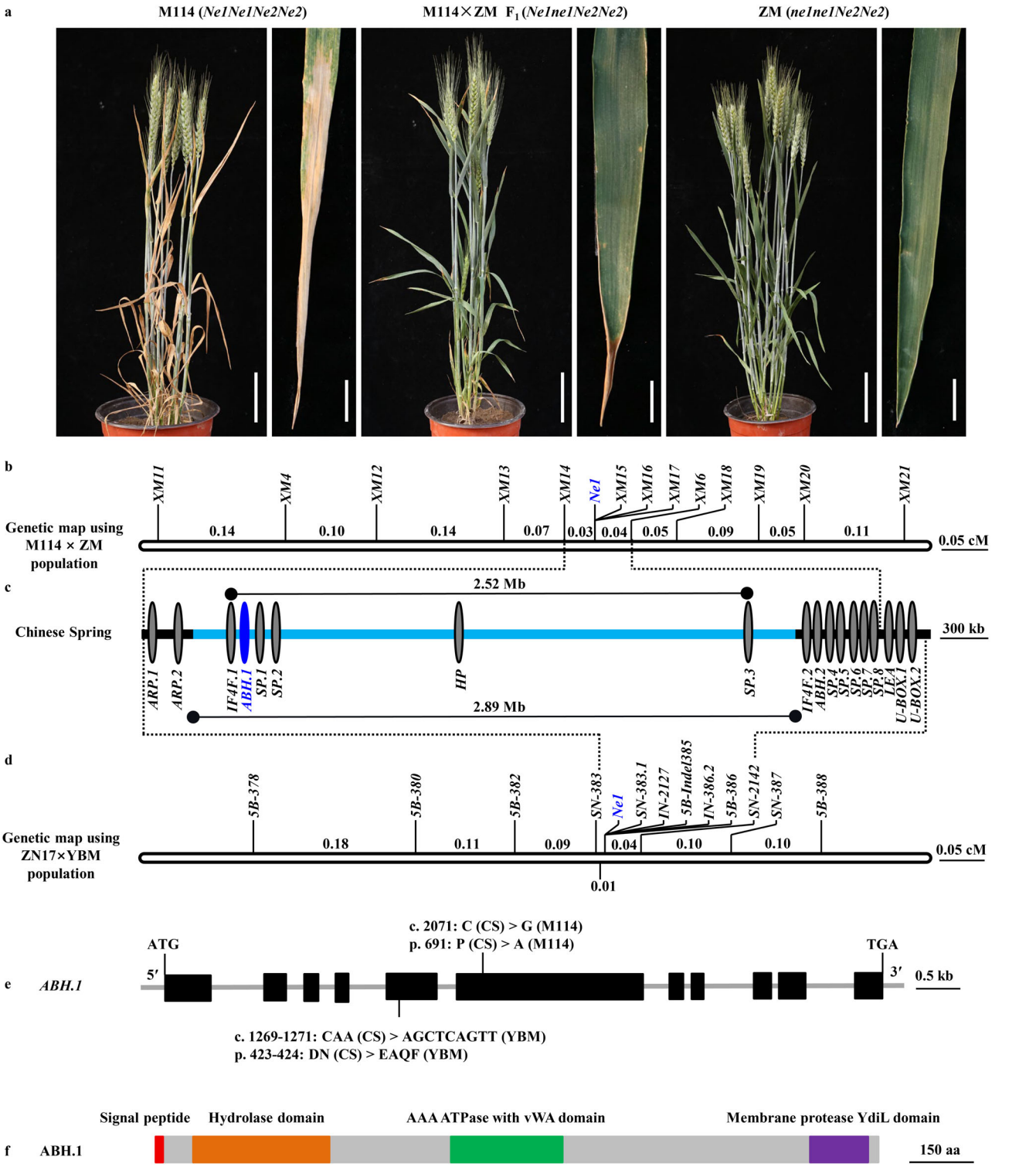

Fig. 1 | Map-based cloning of *Ne1*. **a** Phenotypes of necrotic line M114 (*Ne1Ne1Ne2Ne2*), Zhoumai22 (ZM, *ne1ne1Ne2Ne2*), and F_1 plant derived from M114 × ZM at the grain filling stage in the field. Scale bar in plant, 8 cm; Scale bar in leaf, 2 cm. **b** Fine genetic map of *Ne1* constructed using the F_2 populations derived from M114 × ZM. **c** Physical map of *Ne1* region according to Chinese Spring (CS) reference genome sequence IWGSC RefSeq v2.1. The blue oval indicates *Ne1*. **d** Fine genetic map of *Ne1* constructed using segregation populations derived from Zhengnong17 (ZN17, *ne1ne1Ne2Ne2*) and Yangbaimai (YBM, *Ne1Ne1ne2ne2*). *Ne1* is highlighted in blue. **e** Gene structure and sequence variation of *ABH.1* gene. Black boxes and gray lines indicate exons and introns, respectively. The variation of coding sequence (c) and amino acid (p) sequences between CS, YBM, and M114 are indicated. **f** Protein structure prediction of ABH.1. Hydrolase domain, AAA ATPase with vWA domain, and membrane protease YdiL domain are represented in orange, green, and purple, respectively. The signal peptide is indicated in red. Source data are provided as a Source Data file.

https://doi.org/10.1038/s41467-025-57750-5

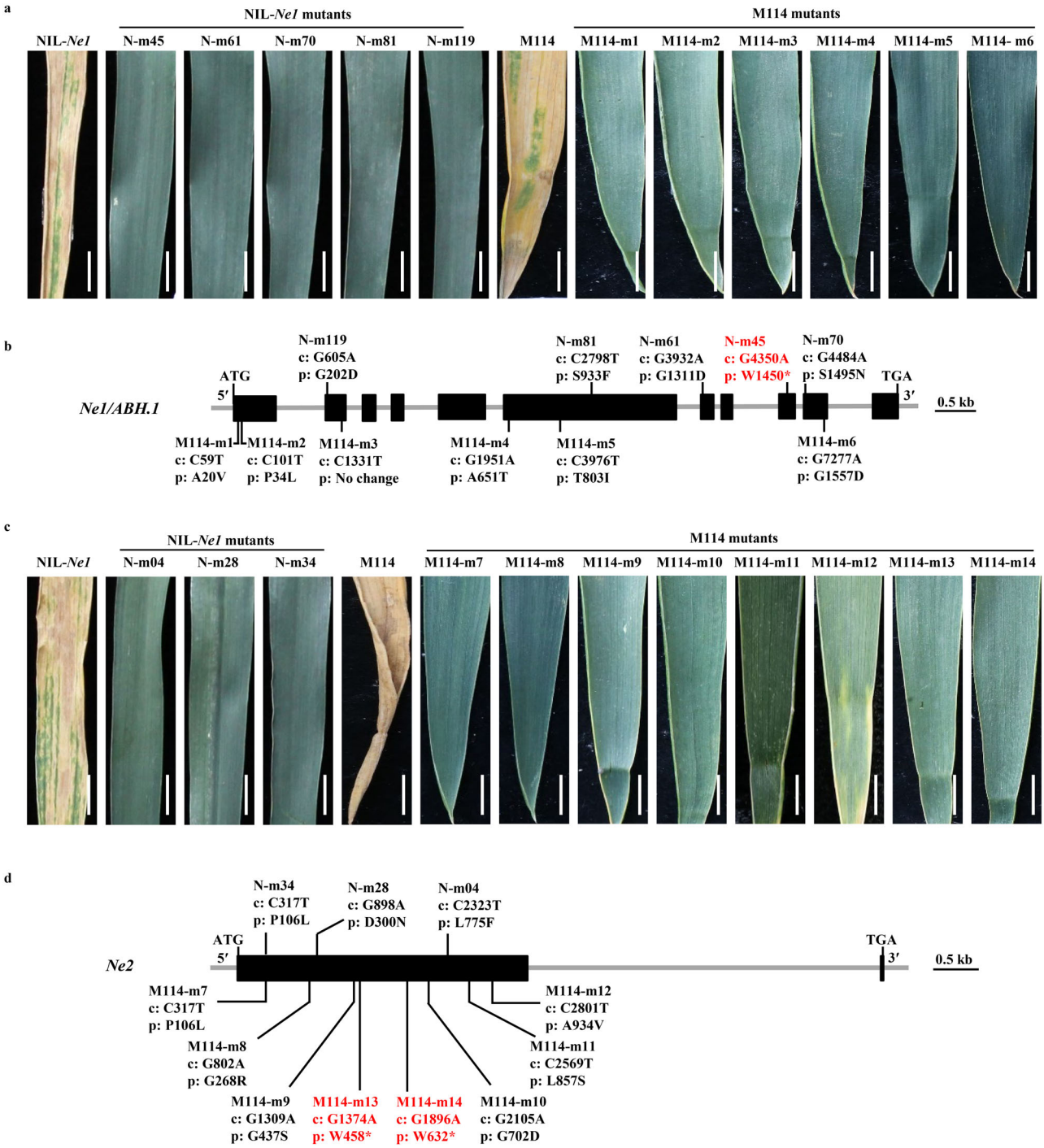

Fig. 2 | Functional validation of *ABH.1* by mutagenesis. a, **c** Phenotypes of non-necrotic mutants generated from the necrotic NIL-*Ne1* (*Ne1Ne1Ne2Ne2*) and M114 (*Ne1Ne1Ne2Ne2*) background by ethyl methanesulfonate (EMS) treatment. Gene structure and EMS mutant analysis of *ABH.1* (**b**) and *Ne2* (**d**). The positions of the EMS-derived loss-of-function mutations are indicated by black lines. Black boxes and gray straight lines represent exons and introns, respectively. The coding sequence (c) changes and their predicted effects on the amino acid (p) are indicated. Scale bar in (**a** and **c**), 1 cm. Mutation names in red indicate nonsense mutations. Source data are provided as a Source Data file.

backgrounds indicated that *ABH.1* is most likely *Ne1*. Furthermore, three NIL-*Ne1*-derived non-necrotic mutants (N-m40, N-m51, and N-m328) did not demonstrate any SNPs in either *Ne2* or *ABH.1*, as well as other genes within the *Ne1* mapping interval, suggesting the presence of mutations in alternative unknown regulators of the necrosis pathway associated with *Ne1-Ne2*.

To further validate the function of *ABH.1*, we performed multiple gene complementation tests with the $ABH.1^{YBM}$ and $ABH.1^{M114}$ alleles, respectively. We amplified the full-length coding region of *ABH.1* from YBM and constructed an overexpression construct, *proUbi*::$ABH.1^{YBM}$ (Fig. 3a). Then, this construct was introduced into the hexaploid wheat cultivar Fielder (*ne1ne1ne2ne2*) using *Agrobacterium*-mediated transformation. All four positive transgenic lines, OE$ABH.1^{YBM}$#1-#4, carrying only $ABH.1^{YBM}$ and not *Ne2*, exhibited normal growth without leaf necrosis (Fig. 3b). To further confirm that $ABH.1^{YBM}$ can induce leaf necrosis in the presence of *Ne2*, we

https://doi.org/10.1038/s41467-025-57750-5

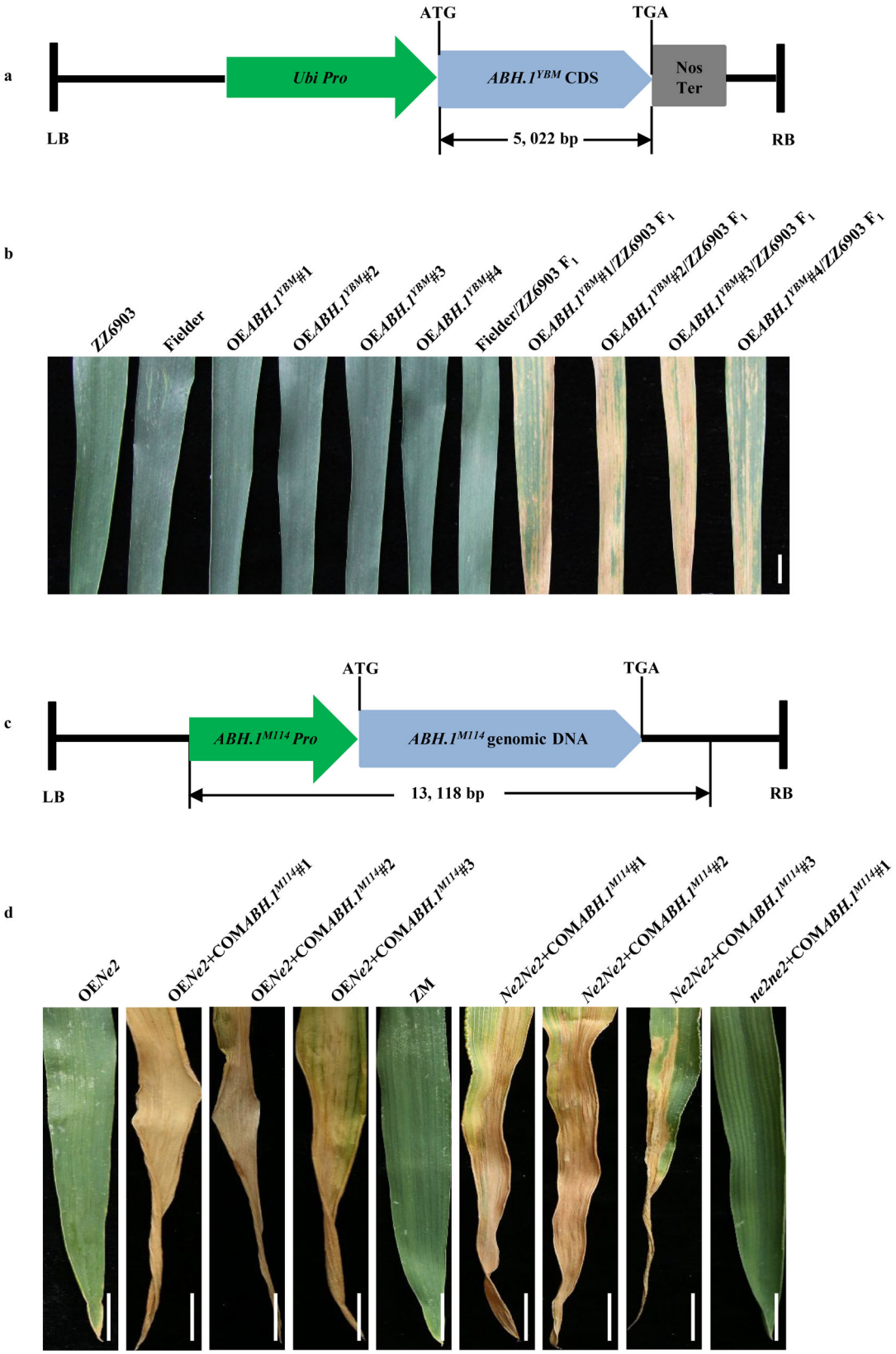

conducted a complementation test by crossing line ZZ6903 (*ne1ne1Ne2Ne2*) with the four homozygous *ABH.1*^{YBM} transgenic lines and Fielder, respectively. The F_1 hybrids derived from Fielder × ZZ6903 displayed normal growth, while all the F_1 hybrids from the crosses between ZZ6903 and *ABH.1*^{YBM} transgenic lines exhibited leaf necrosis (Fig. 3b).

We also generated a construct, *proABH.1*^{M114}::*ABH.1*^{M114}, consisting of a 13,118 bp genomic fragment of *ABH.1*^{M114} from M114, which includes 8157 bp of the entire gene body, 2406 bp of the upstream native promoter, and 2556 bp of the downstream regulatory sequence (Fig. 3c). This construct was transformed into the *Ne2* overexpression transgenic line OE-T_1–1-1 (*ne1ne1ne2ne2Ne2*^{ZM}*Ne2*^{ZM}, hereafter named

Fig. 3 | Transgenic validation of *ABH.1*. **a** Structure of *proUbi*::*ABH.1*^{YBM} used for transformation of wheat cultivar Fielder. The construct contains the *ABH.1*^{YBM} coding sequence (CDS) and maize ubiquitin promoter region (*proUbi*). LB left border; RB, right border; Nos Ter, termination sequence of the *Agrobacterium tumefaciens* nopaline synthase gene. **b** Genetic complementation of *ABH.1* and *Ne2* was performed by crossing independent transformants (OE*ABH.1*^{YBM}#1-#4) carrying *proUbi*::*ABH.1*^{YBM} and wheat cultivar ZZ6903 with the *ne1ne1Ne2Ne2* genotype, which induced the expression of hybrid necrosis. Representative leaves of four F_1 hybrids and their corresponding parental lines are presented. Scale bar, 1 cm. **c** Structure of *proABH.1*^{M114}::*ABH.1*^{M114} used for transformation of the *Ne2* overexpression transgenic line OE-T_1–1-1 (*ne1ne1Ne2Ne2*, OE*Ne2*) in the Fielder genetic background and the F_1 plants (*ne1ne1Ne2ne2*) of ZM × Fielder, respectively, by *Agrobacterium*-mediated transformation. The construct *proABH.1*^{M114}::*ABH.1*^{M114} consisted of a 13,118 bp genomic fragment of *ABH*^{M114} from M114, comprising 8157 bp the entire gene body, 2406 bp upstream native promoter and 2,556 bp downstream regulatory sequences, respectively. **d** Phenotypes of OE*Ne2*, positive transgenic lines (OE*Ne2* + COM*ABH.1*^{M114}#1-#3) in OE*Ne2* background, ZM, positive transgenic lines (*Ne2Ne2* + COM*ABH.1*^{M114}#1-#3, and *ne2ne2* + COM*ABH.1*^{M114}#1) in ZM × Fielder background. Scale bar, 1 cm. Source data are provided as a Source Data file.

OE*Ne2*), in the Fielder genetic background[23] and the F_1 plants (*ne1ne1Ne2ne2*) of the ZM × Fielder cross, respectively, using *Agrobacterium*-mediated transformation. We obtained 10 and 8 positive T_0 transgenic individuals with the confirmed *ABH.1*^{M114} transgene sequence from OE*Ne2* and ZM × Fielder transformation events, respectively. The positive T_0 individuals were advanced to produce T_1 and T_2 generations. T_2-positive transgenic plants carrying *ABH.1*^{M114} in the OE*Ne2* transformation event exhibited pronounced necrosis at the grain filling stage, while OE*Ne2* exhibits slight chlorosis at the leaf tip (Fig. 3d). Similarly, in the ZM × Fielder transformation events, T_2-positive transgenic plants carrying *ABH.1*^{M114} exhibited leaf necrosis when homozygous for *Ne2Ne2* (Fig. 3d), while displaying normal leaves when homozygous for *ne2ne2* (Fig. 3d). The results from multiple independent EMS non-necrotic mutants and transgenic experiments confirm that *ABH.1* is indeed *Ne1*.

ABH.1 triggers hybrid necrosis with *Ne2* by activating immune responses

To better understand the function of *ABH.1*, we investigated its expression patterns by reverse transcription quantitative PCR (RT-qPCR). The results indicate that *ABH.1* is expressed across all tissues examined, with the highest expression level in the leaf blade and comparatively lower level in the young stem and spike (Supplementary Fig. 4a). The necrotic syndrome, which closely resemble a hypersensitivity response (Supplementary Fig. 1), along with the identity of *Ne2* that is the high-temperature leaf rust resistance gene *Lr13*[23], suggest a possible link between hybrid necrosis and immune response. Expression analysis of pathogen-related genes, including *PR1*, *PR2*, *PR3*, *PR5*, and *LOX2*, revealed significant differential expression between near-isogenic lines NIL-*ne1* and NIL-*Ne1* (Supplementary Fig. 4b). Furthermore, the levels of salicylic acid (SA) and jasmonic acid (JA), two well-known phytohormones involved in plant immune responses, were significantly higher in NIL-*Ne1* compared to NIL-*ne1* (Supplementary Fig. 4c). These findings imply a role for autoimmunity activation in the initiation of hybrid necrosis.

The *ABH.1* gene encodes alpha/beta-hydrolases comprising 1671 amino acids, featuring a predicted signal peptide spanning initial residues 1 to 17 (Supplementary Fig. 5a). Both the yeast signal peptide secretion assay and the 2,3,5-triphenyltetrazolium chloride (TTC) staining assay suggest that the predicted signal peptide within ABH.1 may have the potential secretory capability (Supplementary Fig. 5b). To investigate the subcellular localization of ABH.1, we performed co-transfection of *Nicotiana benthamiana* leaves with the *pro35S*::*ABH.1-GFP* construct and the plasma membrane-specific marker *pro35S*::*PIP2-mCherry*[32]. The co-localization of ABH.1-GFP with the PIP2-mCherry marker indicates that ABH.1 is mainly localized to the plasma membrane (Supplementary Fig. 6a, b). In addition, Ne2 is predominantly localized to the cytoplasm and nucleus (Supplementary Fig. 6c).

Allelic and copy number variation effects of *ABH.1* on hybrid necrosis

To investigate the sequence variation of *ABH.1*, we conducted a haplotypic analysis using whole-genome re-sequencing data from 540 hexaploid[33–35] (Supplementary Data 5) and 157 tetraploid[35–37] (Supplementary Data 6) wheat accessions. Seven haplotypes (Hap1-Hap7) were identified (Fig. 4a), and 366 wheat accessions lacked *ABH.1* (Hap0) (Supplementary Data 5 and 6). Notably, although classified as haplotype Hap5, Ripper and Hallam displayed multiple heterozygous SNPs in the intronic regions of *ABH.1* when compared to Mania (Supplementary Fig. 7a). Thus, we speculate that there may be additional copy number variations or structural variations within the *NE1* locus. We then investigated structural variations at the *NE1* locus using whole-genome re-sequencing data from 540 hexaploid wheat[33–35] and identified four structural variations, Zhengnong17-like (ZN17-like, 310 accessions), Yangbaimai-like (YBM-like, 192 accessions), Youzimai-like (YZM-like, 29 accessions), and Wuyuanmai-like (WYM-like, 9 accessions) (Fig. 4b and Supplementary Data 5). Compared to the ZN17-like, YBM-like, YZM-like, and WYM-like materials harbored 1, 2 and 3 copies of the 2.89 Mb-fragment, respectively (Fig. 4b). Moreover, we also found the multiple 2.89 Mb-fragments in the YZM-like or WYM-like subtype materials are not identical, suggesting the potential presence of complex structural variation within *Ne1* genetic interval (Supplementary Fig. 7b).

Furthermore, we conducted an investigation to determine if *ABH.1* is present in different copies. Utilizing the coverage depth as a criterion, four copy number variations (CNVs) of *ABH.1*, CNV-0, CNV-1, CNV-2, and CNV-3, were identified using whole-genome re-sequencing data from 540 hexaploid wheat[33–35] (Supplementary Data 5). These CNVs correspond to the presence of zero, one, two, or three copies of *ABH.1*, respectively, and they also aligned with four structural variations ZN17-like, YBM-like, YZM-like, and WYM-like, respectively (Fig. 4c). The copy number analysis of *ABH.1* in the eight representative materials confirmed the CNVs of *NE1* locus (Supplementary Fig. 8a and Supplementary Data 7). CNVs play a pivotal role in modulating gene expression and influencing phenotypic diversity[14]. RNA-sequencing data from 305 hexaploid wheat[33] also demonstrated that the expression levels of *ABH.1* were significantly higher in the CNV-2 and CNV-3 accessions relative to the CNV-1 accessions (Fig. 4d and Supplementary Data 8).

Previous reports revealed that there are at least three *Ne1* alleles, *Ne1*^{w}-weak, *Ne1*^{m}-moderate, and *Ne1*^{s}-strong, with diverse effects based on the severity of necrosis observed in F_1 progenies[38]. To illuminate the effects of *ABH.1* alleles, we chose wheat accessions representing different haplotypes of *ABH.1*, including CS (Hap1), YM14 (Hap2), YBM (Hap3), PI 171028 (Hap4), and Mania (Hap5) (Fig. 5a), all of which belong to CNV-1 (Fig. 5b), and crossed them with ZZ6903 (Hap0, CNV-0) with the *ne1ne1Ne2Ne2* genotype. The F_1 hybrids from the crosses of YM14 × ZZ6903 and YBM × ZZ6903 exhibited necrotic symptoms that were similar to, or slightly more severe than, those observed in the CS × ZZ6903 cross (Fig. 5c, d). CS is previously believed to carry *Ne1*^{w} allele[6]. Therefore, Hap1, Hap2, and Hap3 of *ABH.1* could correspond to *Ne1*^{w} allele. The F_1 hybrids from the crosses PI 171028 × ZZ6903 and Mania × ZZ6903 displayed an extremely severe necrotic symptom, leading to complete leaf desiccation and death at the flowering stage (Fig. 5d) and resulting in very small seeds. These findings suggest that Hap4 and Hap5 of *ABH.1* could correspond *Ne1*^{s} allele.

https://doi.org/10.1038/s41467-025-57750-5

a

Position	85	394	796	1165-1170	1269-1271	1783	2071	3601	4024	4386	Representative variety	No.
A.A. Sub	V 29 F	K 132 E	Q 266 E	RR 389-390 -	DN 423-424 EAQF	D 595 N	P 691 A	E 1201 K	D 1342 N	D 1462 E		
Hap1	G	A	C	CGTCGT	CAA	G	C	G	G	T	CS	119
Hap2	G	A	C	CGTCGT	CAA	G	G	G	G	T	YM14	66
Hap3	G	A	C	CGTCGT	AGCTCAGTT	G	C	G	G	T	YBM	1
Hap4	T	G	G	-	CAA	G	C	G	A	G	PI 171028	1
Hap5	T	A	C	-	CAA	G	C	G	G	G	Mania	79
Hap6	T	A	C	-	CAA	A	C	G	G	G	PI 272572	6
Hap7	T	G	C	-	CAA	G	C	A	G	G	PI 585017	59

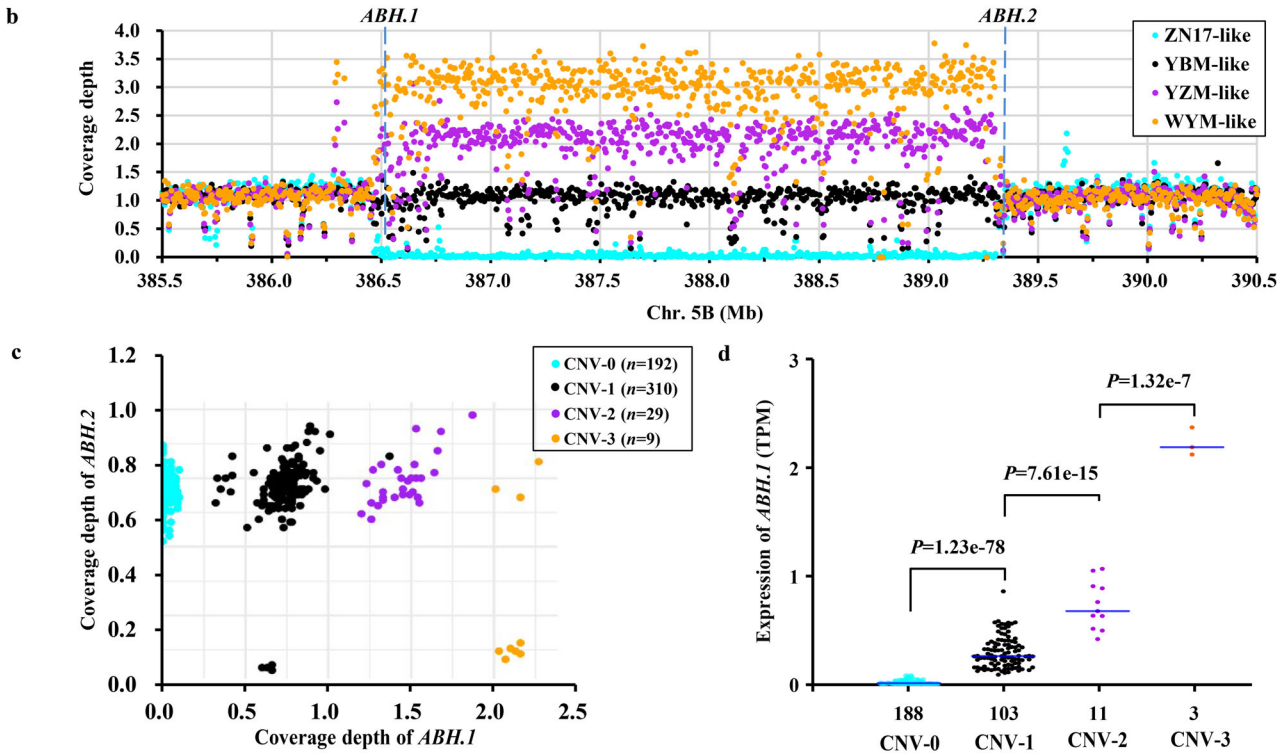

Fig. 4 | Allelic and copy number variation of *ABH.1*. **a** Haplotype analysis of *ABH.1* using whole-genome re-sequencing data from 540 hexaploid and 157 tetraploid wheat accessions. Variants at the coding sequence of *ABH.1* were clustered into seven major haplotypes (Hap1-Hap7), while 366 accessions lacked *ABH.1* (Hap0). Introns and exons are represented by lines and black boxes, respectively. The coding nucleotide and amino acid sequences of Chinese Spring (CS) are shown in black font, and the bracketed numbers represent the relative positions of nucleotide or amino acid sequences concerning ATG or Met, respectively. Deletions are indicated by the symbol '-'. YM14, Yumai14; YBM, Yangbaimai. **b** Four major representative structural variations of the *NE1* locus. Reads from these wheat samples were aligned to the Chinese Spring reference genome sequence IWGSC RefSeq v2.1, and coverage depth for each 5 kb window was computed. The coverage depth for each 5 kb window was then normalized based on the total coverage depth. Finally, the normalized depth for the target region (Chr5B:385.5-390.5 Mb) was presented in the form of a scatter plot, with each data point representing a 5 kb window. **c** Coverage depth of the *ABH.1* gene in the published re-sequence dataset for 540 hexaploidy wheat accessions. The *ABH.2* (*TraesCS5B03G0565000*) gene is situated downstream of *ABH.1* (*TraesCS5B03G0561800*), with the sequencing coverage depth of *ABH.2* used as an indicator of normal resequencing outcomes within this genomic region. Reads from wheat samples were aligned to the Chinese Spring RefSeq v2.1, and coverage depth was determined for each gene. The coverage depth for each gene was subsequently normalized by the total coverage depth, and the resulting normalized depth for the target gene was depicted in a scatter plot, with each data point representing a specific wheat accession. The *n* number is the sample size used to derive statistics. **d** The expression of *ABH.1* was compared among the four CNV (copy number variation) groups (two-sided Student's *t* test; centerline, median). RNA-seq data from 305 common wheat genomes (one biological replicate) were used to quantify *ABH.1* expression for the four CNV groups. *P*-values are shown at the top of data points, and *n*, the sample size used to derive statistics, is listed at the bottom of the figure. TPM, transcripts per million. Source data are provided as a Source Data file.

To further investigate whether CNVs of *ABH.1* also affect necrosis in addition to haplotypes of *ABH.1*, we utilized PI 182704, Ripper, and Hallam, which are belong to Hap5 and the CNV-3, cross with ZZ6903, respectively (Fig. 5a, b). The F_1 plants from the crosses PI 182704 × ZZ6903, Ripper × ZZ6903, and Hallam × ZZ6903 exhibited exacerbated necrosis and significantly reduced seed production compared to those from Mania × ZZ6903 (Fig. 5d, e). RT-qPCR analysis confirmed that the transcript levels of *ABH.1* are significantly higher in

https://doi.org/10.1038/s41467-025-57750-5

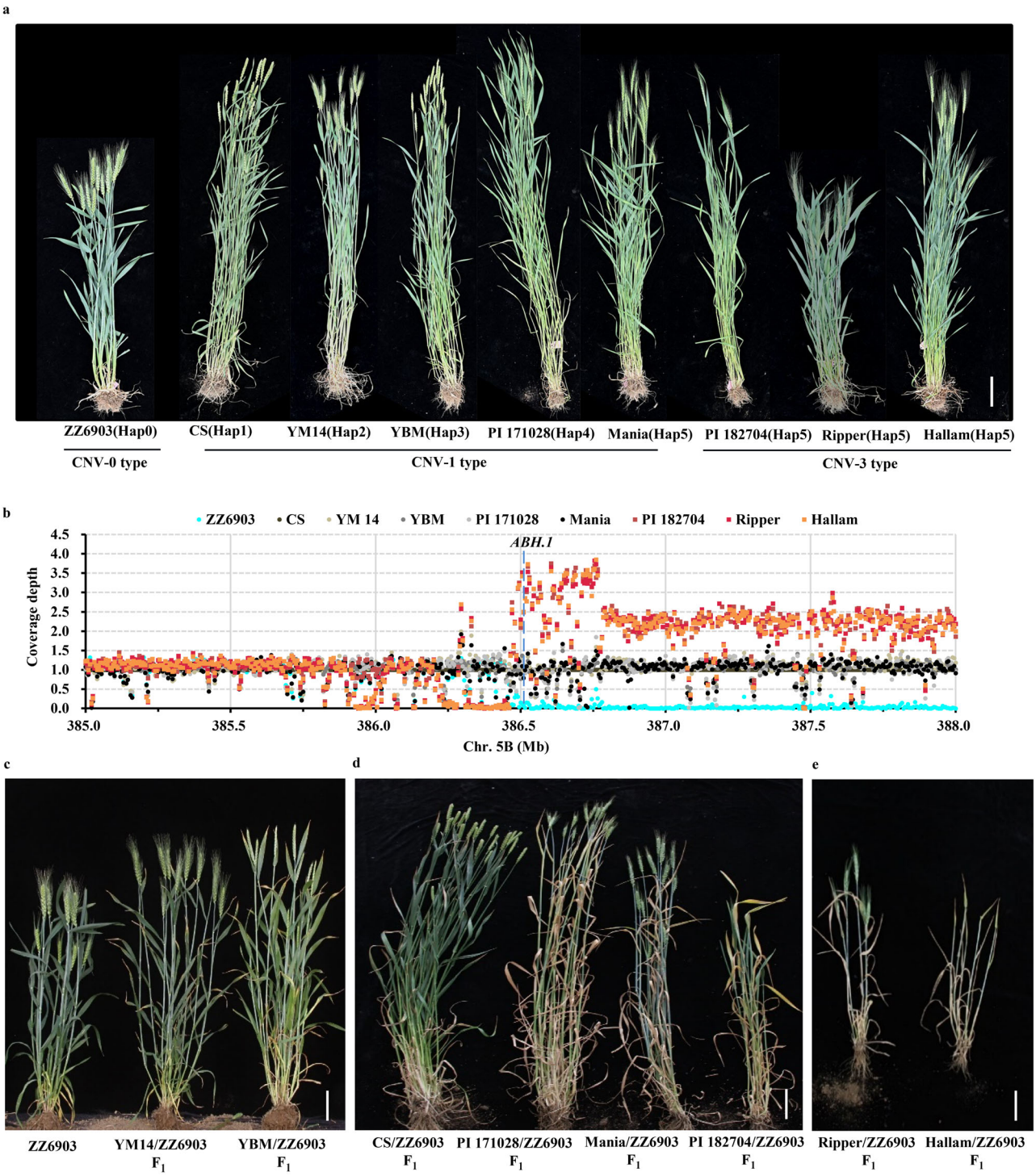

Fig. 5 | Effects of allelic and copy number variations at *ABH.1* locus on hybrid necrosis. a Phenotypes of a series of materials carrying different *ABH.1* alleles. Scale bar, 10 cm. **b** Structural variations of the *ABH.1* locus from materials carrying different *ABH.1* alleles. **c**–**e** Phenotypes of ZZ6903, and the representative F_1 plants derived from crosses between wheat accessions (carrying *ne2ne2* and different *ABH.1* haplotypes) × ZZ6903 (*ne1ne1Ne2Ne2* genotype). ZZ6903, Zhengzhou 6903; YM14, Yumai 14; YBM, Yangbaimai; CS, Chinese Spring. Scale bar in plant, 10 cm. Source data are provided as a Source Data file.

the leaves of PI 182704, Ripper, and Hallam relative to Mania (Supplementary Fig. 8b). These findings suggest that both allelic and copy number variations of *ABH.1* contribute to hybrid necrosis.

Evolutionary trajectory of *ABH.1*

Phylogenetic analysis revealed that orthologous genes of *ABH.1* are widely present across gramineous plants (Supplementary Fig. 9). To investigate the evolutionary origins of *ABH.1*, we conducted a homologous analysis of *ABH.1* in nine Sitopsis genomes[39,40] and 157 re-sequenced tetraploid genomes[35–37]. Our results indicated that *ABH.1* is absent in nine Sitopsis species (Supplementary Fig. 10). However, multiple haplotypes of *ABH.1* and the four CNVs of *ABH.1* were observed in tetraploid wheat species, including *Triticum durum* and *Triticum dicoccoides* (Supplementary Fig. 11 and Supplementary

https://doi.org/10.1038/s41467-025-57750-5

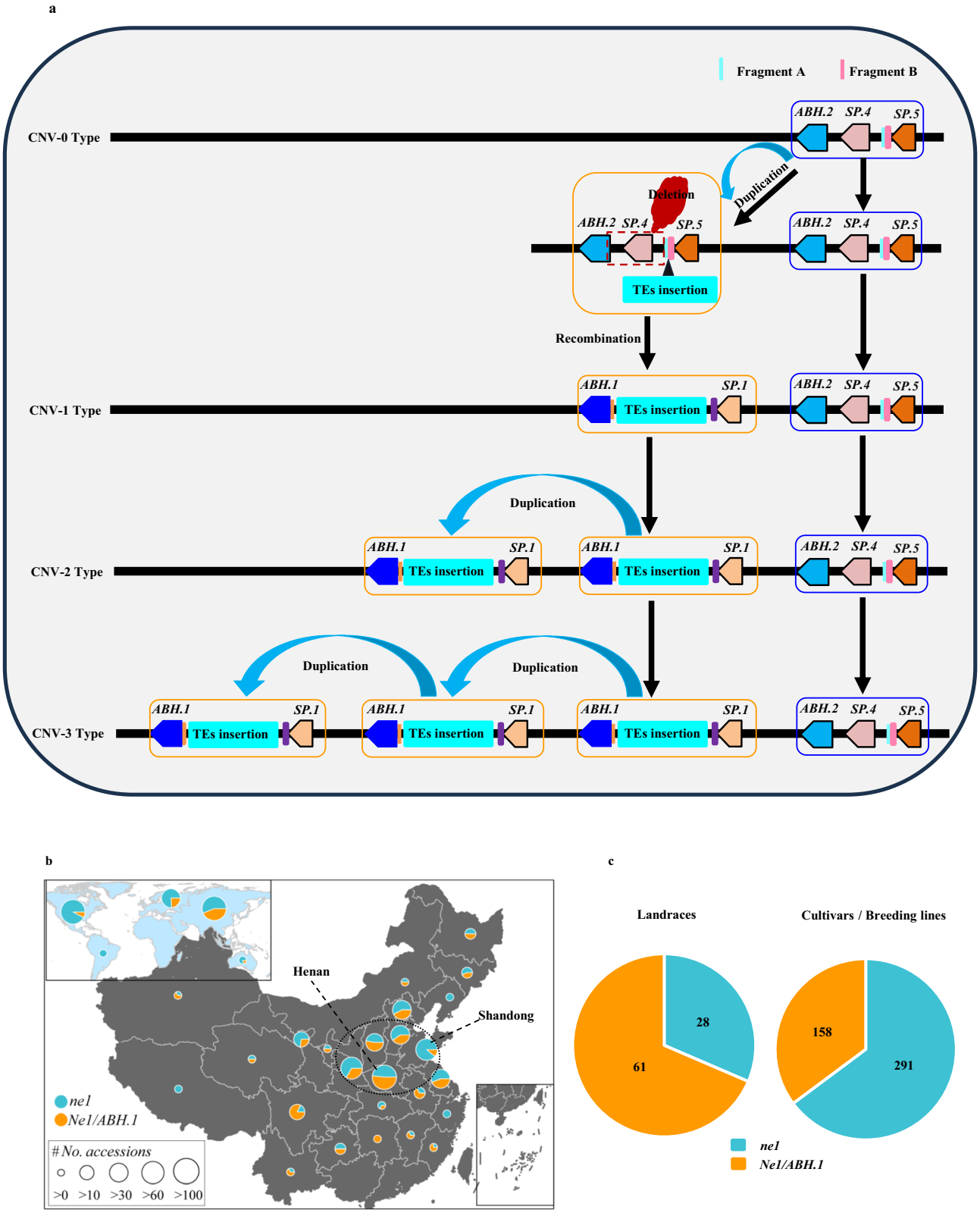

Data 6). These findings suggest that *ABH.1* likely originated from wild emmer wheat.

ABH.1 has homologs in the A, B, and D sub-genomes of CS (Supplementary Fig. 9). Comparative genomic analysis demonstrated significant structural variation at *NE1* locus, in contrast to the corresponding homologous regions in the A and D sub-genomes (Supplementary Fig. 12a). However, the *NE1* locus exhibits good micro-collinearity within the homologous regions of the A, B and D sub-genome in hexaploid wheat Fielder, carrying the *ne1* allele (Supplementary Fig. 12b). Genomic sequence comparison of *Ne1* genetic interval between CS and Fielder indicate that the 2.89 Mb insertion fragment shares a strong similarity with the adjacent genomic region spanning from *IF4F.2* to *SP.8* (Supplementary Fig. 12c), suggesting this region may have resulted from duplication and ectopic recombination events.

Fig. 6 | Evolutionary trajectory and distribution of *ABH.1*. **a** A proposed model for the evolutionary trajectory of *ABH.1*. Following a segmental duplication event encompassing the genomic loci of *ABH.2*, *SP.4*, and *SP.5*, designated as CNV-0 type, there was a subsequent deletional event within the duplicated segment. This resulted in the loss of the entire *SP.4* gene sequence, as well as the promoter region and the initial 315 base pairs of the first exon of the *ABH.2* gene. Subsequently, transposable elements (TEs) were inserted into the 3′ downstream region of the *SP.5* gene, situated between Fragment A and Fragment B. The integration of these TEs with a segment of the downstream sequence of the *SP.5* gene, in conjunction with the truncated remnant of the *ABH.2* gene, catalyzed the genesis of a novel functional gene entity, characterized as the *ABH.1* gene (CNV-1 type). As a hotspot for genomic recombination, this region has also undergone events resulting from one (CNV-2 type) and two (CNV-3 type) duplications. **b** Global distribution of *Ne1/ABH.1* and *ne1* alleles in a worldwide wheat collection ($n = 853$). Samples were categorized into *Ne1/ABH.1* allele type and *ne1* allele type based on their genetic type in the *NE1* locus, and the proportions of samples in different regions were represented using pie charts. Initially, the geographic coordinates of the samples were imported as point layers and overlaid with corresponding national and continental boundary data. Subsequently, pie charts were added at the sampling locations in each region, with different colors representing distinct haplotype categories and the size of the pie charts reflecting the total number of samples in that region. **c** *Ne1/ABH.1* allele was negatively selected in Chinese wheat breeding. A total of 89 landrace wheat and 449 cultivar wheat accessions were used to investigate the distribution of *Ne1/ABH.1* and *ne1* alleles. Source data are provided as a Source Data file.

The *ABH.2* gene, which is located downstream of the 2.89 Mb insertion fragment within *Ne1* genetic interval, shares an 92.83% identity in amino acid sequences with *ABH.1* (Fig. 1c). ABH.1 differs from ABH.2 by lacking the initial 105 N-terminal amino acids and instead possesses an additional signal peptide of 17 amino acids (Supplementary Figs. 5, 13 and 14), which is unique to the orthologs of ABH.1 in cereal species (Supplementary Fig. 15). Sequence analysis identified multiple transposable elements (TEs) within the promoter region of *ABH.1* (Supplementary Fig. 16). Interestingly, a 377 bp sequence of the 5′-end upstream region and 57 bp sequence of the first exon of *ABH.1* show a 93.58% identity to the 3′-downstream region of *SP.5* (Supplementary Fig. 17), which is the homolog of *SP.1*. Further analysis of the 3′-downstream sequence of *SP.5* revealed that two adjacent fragments, designated as Fragment A and Fragment B, align with the 5′-end of *ABH.1* and the 3′-downstream part of *SP.1*, respectively. Two fragments are separated by TEs (Supplementary Fig. 17).

Consequently, we propose a hypothetical evolutionary trajectory for *ABH.1* (Fig. 6a). Following the segmental duplication containing genes *ABH.2*, *SP.4*, and *SP.5*, the entire gene *SP.4*, along with the promoter region and the first exon (315 bp) of *ABH.2*, was lost from the duplicated segment. Subsequently, TEs were inserted into the 3′-downstream region of gene *SP.5*. These transposons were then fused with a part of the downstream sequence of gene *SP.5* and the truncated gene *ABH.2* to create a new functional gene *ABH.1*.

Distribution of *ABH.1*

We utilized the diagnostic markers *Ne1-Select2128* for *Ne1* and *Ne2-Select91* for *Ne2* to screen a globally sourced diverse panel of tetraploid and hexaploid wheat (Supplementary Fig. 18). The results show that the presence proportion of *Ne1* is 62.5% (120/192) in wild emmer wheat, 26.0% (52/200) in cultivated emmer wheat, 81.3% (156/192) in durum wheat, and 38.7% (330/853) in hexaploid wheat. However, *Ne2* is not present in any of the tetraploid wheat tested, and its presence proportion in hexaploid wheat is 5.9% (50/853) (Supplementary Data 9 and 10). The frequency of *ABH.1* in North American common wheat is significantly lower than that observed in Europe and Asia (Fig. 6b). The geographic distribution of *ABH.1* in the central wheat region of China shows the highest frequency (51.76%) in Henan province, and the lowest (11.27%) in Shandong province (Fig. 6b). Geographic distribution analysis of Chinese common wheat revealed the frequency of *ABH.1* is significantly lower in modern cultivars and breeding lines than in landrace (Fig. 6c), indicating that *ABH.1* was negatively selected in Chinese wheat breeding.

Discussion

Wheat hybrid necrosis, mediated by the complementary genes *Ne1* and *Ne2*, was first reported in 1921[19]. The *Ne2* gene was characterized as an NLR immune receptor[22–24]. Here, we successfully isolated *Ne1*, encoding an ABH protein, through map-based cloning, mutagenesis, and transgenic approaches. Furthermore, we found that the *Ne1* allele likely originated from wild emmer wheat, potentially arising from segmental duplication and ectopic recombination. Notably, haplotypic and structural variations that altered the *Ne1* gene expression are driving forces of hybrid necrosis diversification in wheat. This study sheds light on the long-standing mystery of *Ne1-Ne2* interaction-induced hybrid necrosis in wheat. The *Ne1-Ne2* (*ABH.1-NLR*) mediated necrosis in wheat reveals a parallel conserved function to the interaction of *DM2-DM3* (*NLR-ABH*), which are involved in innate immunity and hybrid necrosis in *Arabidopsis*[3,30,31].

Hybrid necrosis is often associated with an autoimmune response[1]. The genetic combination of *Ne1* and *Ne2* results in necrosis. However, when only *Ne2* is present, it does not exhibit necrotic symptoms but does confer resistance to leaf rust[23]. Previous evidence suggests that the presence of *Ne1* may lead to an increase in the expression of *Ne2*[22]. In this study, we found that compared to NIL-*ne1*, the levels of pathogenesis-related genes expression and phytohormones, salicylic acid, and jasmonic acid in NIL-*Ne1* are higher (Supplementary Fig. 4b, c), suggesting that *Ne1* may be involved in autoimmunity activation. Similar results have been also observed in rice hybrid weakness mediated by *Hwi1* and *Hwi1*. The activation of some *PRs*, such as *PBZ1*, was always associated with the occurrence of weakness syndrome under various conditions. Salicylic acid and jasmonic acid were highly accumulated in NIL(*Hwi1*) basal nodes[9].

Gene duplication drives genome and genetic system evolution, facilitating functional diversification[14]. Our findings suggest that the 2.89 Mb insertion fragment containing *ABH.1* likely formed through duplication and ectopic recombination events (Supplementary Fig. 12c). Multiple segmental duplications among hexaploid and tetraploid wheat indicated a duplication hotspot at *NE1* locus (Fig. 6a). Notably, the YZM-like subtype materials harbors two 2.89 Mb insertion fragments; however, a segregation in heterozygosity is observed, which implies the potential presence of complex structural alterations within *Ne1* genetic interval (Supplementary Fig. 7b). The similar situation was detected in the WYM-like subtype materials, which carries three 2.89 Mb insertion fragments (Supplementary Fig. 7b). Variations in gene copy number can alter the level of gene expression, thereby affecting traits[14]. Our results demonstrated that the expression level of *ABH.1* was significantly higher in the CNV-2 and CNV-3 accessions relative to the CNV-1 accessions (Fig. 4d). Genetic experiments demonstrate that both allelic and copy number variation of *ABH.1* contributes to hybrid necrosis.

Gene rearrangement, duplication, and fusion have the potential to create new genes. *ABH.1* and *ABH.2* are both located in the genetic interval of *Ne1* and share 92.83% protein sequence similarity. Compared to ABH.2, ABH.1 misses the first 105 N-terminal amino acids and contains an additional 17-amino-acid signal peptide that is specific to ABH.1 orthologs in cereal species (Supplementary Figs. 5, 13–15). Sequence analysis reveals that *ABH.1* is likely from gene duplication and ectopic recombination (Fig. 6a). Since the available wheat genome sequence data predominantly belong to the ZN17-like and YBM-like types (Supplementary Fig. 19), no published resequencing data exists for the materials of YZM-like and WYM-like type.

Therefore, the direction of the additional 2.89 Mb fragment in YZM-like and WYM-like materials remains uncertain. With advancements in third-generation sequencing technology, this ambiguity may be resolved in the future. In our genetic experiments, the F_1 hybrids derived from the cross PI 171028 × ZZ6903 exhibited necrosis symptoms (Fig. 5d). However, PI 171028, which carries the *ABH.1*, lacks the *ABH.2* (Supplementary Fig. 20). In contrast, the F_1 hybrids of ZZ6903 and ZN17, an accession lacked *ABH.1* and shared the identical *ABH.2* gene sequence of YBM (Supplementary Fig. 20), showed normal growth. Therefore, despite the high protein sequence identity between ABH.1 and ABH.2 (Supplementary Fig. 14), ABH.2 is not involved in wheat hybrid necrosis, suggesting that *ABH.1* is a neofunctionalization gene.

In this study, among 58 *T. dicoccoides* wheat accessions primarily from Israel (36), Lebanon (6), Syria (8), and Turkey (6), CNV-0 and CNV-1 types were detected. However, CNV-2 and CNV-3 types were prevalent in cultivated emmer wheat subspecies (Supplementary Data 6). Further investigation is needed to determine the presence or absence of CNV-2 and CNV-3 in wild emmer wheat using more accessions.

Moreover, *Ne2* was absent in all tested 584 tetraploid wheat accessions analyzed (Supplementary Data 9). The results suggest that *Ne1* likely originated in wild emmer and integrated into hexaploid wheat through polyploidization, while *Ne2* might be emerged post-hexaploidization or from other wheat relatives.

Wheat hybrid necrosis can hinder gene flow, impacting wheat genetic improvement[38]. The *Ne1* functional marker *Ne1-Select2128*, combined with *Ne2-Select91*, a diagnostic marker for *Ne2*[22], can detect both *Ne1* and *Ne2* in a single PCR reaction (Supplementary Fig. 18b). Our findings indicate that none of the tested materials simultaneously carry both *Ne1* and *Ne2* (Supplementary Data 9 and 10), likely due to their detrimental interaction. The *Ne2*, which is identical to the leaf rust resistance gene *LrZH22*/*Lr13* in the elite cultivar Zhoumai 22[23], has experienced positive selection, while negative selection was observed for *Ne1* (Fig. 6c). The positive selection for *Ne2*/*LrZH22*/*Lr13* during breeding has significantly increased the frequency of the *ne1* allele in modern breeding varieties. Cultivars like Andes, Chris, Ciano 67, and Pavon 76, which carry *Lr13*, were extensively used as leaf rust resistance sources in CIMMYT's wheat breeding program[41,42]. The pleiotropic nature of the *Lr13* and *Ne2* genes may have contributed to the increased prevalence of *Ne2* in US wheats (Fig. 6b), crowding out *Ne1* and sharply reducing its proportion. The presence of *Ne2*/*Lr13* in elite wheat varieties like Liangxing 99, Yannong 15, and Jimai 22 possibly explains the high frequency of the *ne1* allele in wheat varieties of Shandong province[23] (Fig. 6b).

Methods

Plant materials and growth conditions

The common wheat line M114 carries both *Ne1* and *Ne2*, while Zhoumai 22 (ZM) is a commercially elite cultivar with *Ne2*[23]. We utilized an F_2 population derived from M114 × ZM for fine mapping *Ne1*, with subsequent phenotypic verification conducted on F_3 progenies of key F_2 recombinants within the *Ne1* genetic interval. In another fine mapping population for *Ne1*, we constructed recombinant inbred lines from common wheat Zhengnong 17 (ZN17, *ne1ne1Ne2Ne2*) × Yangbaimai (YBM, *Ne1Ne1ne2ne2*) and Zhengzhou 6903 (ZZ6903, *ne1ne1-Ne2Ne2*) × Yumai 14 (YM14, *Ne1Ne1ne2ne2*)[26]. RIL-368 (*Ne1ne1Ne2Ne2*) is a residual heterozygous line at the *NE1* locus derived from the F_8 recombinant inbred lines of the ZN17 × YBM cross. Aside from exhibiting differences in normal and necrotic phenotypes, RIL-368 does not display any significant visible variations. Therefore, we self-pollinated RIL-368 to generate nearly isogenic lines: NIL-*ne1* and NIL-*Ne1*. To genetically verify the effect of the *Ne1* allele, ZZ6903 was crossed with different wheat accessions (Mania, Chinese Spring, PI 171028, PI 182704, Hallam, and Ripper). A collection of 584 accessions of tetraploid wheat (Supplementary Data 9), and 853 accessions of hexaploid wheat (Supplementary Data 10) was used to determine *Ne1* alleles. All these plant materials were planted in 1.5 m rows with 30 cm row spacing, leaving ~14 cm between each plant, at the experimental fields of the Institute of Genetics and Developmental Biology, Chinese Academy of Sciences, in Shijiazhuang, Hebei province, China.

The transgenic experiments involved the use of common wheat cultivar Fielder, homozygous *Ne2* overexpression transgenic line OE-T_1–1-1 (OE*Ne2*)[23], and the F_1 hybrid plants from Fielder × ZM. All plants for transgenic experiments were cultivated in pots (20 cm × 20 cm) in a greenhouse with a 16 h-light/8 h-dark cycle (25 °C/18 °C, 65% relative humidity) at the Institute of Genetics and Developmental Biology, Chinese Academy of Sciences, Beijing, China. Supplementary Data 1 presents the genotypes at the *NE1* and *NE2* locus for the wheat materials mentioned in this study.

Phenotyping

Wheat plants, including the parents, F_1, F_2, $F_{2:3}$ families, EMS mutants, and transgenic plants, were evaluated for leaf necrosis at the grain-filling stage under field conditions or controlled greenhouse. Plants with complete necrotic death of flag leaf and leaves below it were scored as necrosis and those with all normal flag leaves and leaves below it were scored as non-necrotic. The Pearson's Chi-squared (χ^2) tests were performed to determine the fitness of segregation ratios to theoretical Mendelian ratios using the SAS 8.0 statistical analysis package (SAS Institute, Cary, NC, the United States).

Histochemistry

Accumulation of H_2O_2 at the site of lesion formation in NIL-*Ne1* was visualized by DAB staining as previously described with minor modifications[43]. Specifically, at the flowering stage, when the necrotic area of the flag leaves of NIL-*Ne1* plants was approximately 5–10%, whole flag leaf blades of both NIL-*Ne1* and NIL-*ne1* plants were collected. The entire leaves were then immersed in 1 mg/mL DAB staining solution for 24 h, followed by decolorization in a chloral hydrate solution for another 24 h, and rinsed twice with distilled water. Photographs were taken using a digital camera, and the staining intensities were compared. The experiment was conducted three times, each time using flag leaves from six NIL-*Ne1* plants and six NIL-*ne1* plants.

BSR-Seq analysis

In the bulked segregant RNA-sequencing (BSR-Seq) experiment[44], the flag leaves from 50 homozygous necrotic and 50 homozygous normal F_3 families from M114 × ZM at the flowering stage, represented by an equal amount of leaf tissues from single plants of each line, were collected randomly to compose the necrotic and normal RNA bulks for RNA-Seq. RNA samples were extracted using the TRIzol protocol (Tiangen, Beijing, China, Catalog No. DP424) and sequenced on an Illumina HISeq 4000 platform by Beijing Novogene Bioinformatics Technology Co. Ltd, Beijing, China, following the manufacturer's standard protocol. The clean reads were aligned against the Chinese Spring reference genome sequence IWGSC RefSeq v2.1[29] using STAR software with default parameters[45]. SNP calling was conducted using GATK software[46], with a filtration criterion of allele frequency difference (AFD) > 0.8 and Fisher's Exact Test *P*-value < 1e-10.

Marker development and linkage analysis

Based on the BSR-Seq results, SNPs and InDels associated with *Ne1* were selected for marker development and validation. The flanking sequences, approximately 3 kb, of the associated SNPs and InDels were identified from the Chinese Spring reference genome IWGSC RefSeq v2.1[29] and used as templates for designing PCR primers using the web-based program available at the GSP website (http://probes.pw.usda.gov/GSP/) to amplify 800-1000 bp sequences containing the variant. Genomic DNA was extracted from young leaves of M114, ZM, 5 homozygous necrotic, and 5 homozygous normal F_3 families using the

cetyl trimethyl ammonium bromide (CTAB) method[47]. PCR was performed in a Biometra T3000 Thermocycler (Applied Biosystems, New York, NY, USA). Each 10 μL reaction mixture comprised 5 μL of PCR mixture (including *Taq* polymerase, dNTPs, and 10× PCR buffer with Mg^{2+}), 2 μL ddH_2O, 1 μL DNA (50 ng μL^{-1}), and 1 μL of 10 μmol L^{-1} each of the forward and reverse primers. The PCR profile included initial denaturation at 95 °C for 3 min; 95 °C for 15 s, annealing at 56–61 °C (depending on the primers used) for 10 s, and 72 °C for 1 min, 35 cycles; and extension at 72 °C for 10 min. The sequences of the primers used are detailed in Supplementary Data 3. Sanger sequencing of the amplicons was performed to validate true polymorphisms (Tsingke, China). The closest SNP markers were used as queries for BLAST against the Chinese Spring whole genome assembly sequences. The genomic sequences in the target genomic region of *Ne1* were used as templates to design SSR primers using $B_{ATCH}P_{RIMER}3$ software (http://batchprimer3.bioinformatics.ucdavis.edu/)[48]. Polymorphic SSR markers between M114 and ZM and the contrasting DNA bulks were used to construct the genetic linkage map of *Ne1* after genotyping the mapping population. Linkage analysis of molecular markers and the *NE1* locus was conducted using the software MAPMAKER 3.0 with a LOD score threshold of 3.0[49].

Mutagenesis and identification of non-necrotic mutants

Seeds of the necrotic line NIL-*Ne1* were subjected to mutagenesis with EMS. A total of 10,000 seeds were incubated in deionized water for seven hours at room temperature, followed by gentle shaking for 12 hours at ambient temperature using 2000 mL of 0.5% EMS (v/v) solution. Following treatment, the seeds underwent an eight-hour rinse under running water and were left to air-dry in the fume hood overnight (~16 h). Subsequently, the EMS-treated M_1 seeds were artificially sown in the field (Hebei, China). Approximately 170 spikes exhibiting a potential reduction of necrotic symptoms were collected from about 6000 M_1 plants based on preliminary visual inspection. A total of 156 independent M_2 families, comprising ~30 plants per plot, were visually screened for non-necrotic mutants.

Non-necrotic mutants were also generated in the necrotic M114 background. Approximately 10,000 seeds of M114 were soaked in water for eight hours, then treated with 0.5% (v/v) EMS solution at room temperature for 16 h followed by washing with running water for 4 h, covered with Whatman paper, and air-dried at 4 °C[50]. EMS-treated M_1 plants were generated at the Gaoyi Experimental Station (Hebei, China). M_2 families (25 seeds per family) were planted in the field for phenotypic investigation. All M_3 seeds obtained from M_2 non-necrotic mutants were planted in the field to confirm the homozygous mutations.

Total RNA was extracted from the flag leaves of homozygous non-necrotic mutants at the flowering stage in the field using a TRIzol reagent (Invitrogen, USA). First-strand cDNA was synthesized utilizing the PrimeScript™ RT reagent Kit with gDNA Eraser (TaKaRa, Japan). The full-length cDNA sequences for *Ne1* candidate genes, as well as *Ne2* in all M_3 homozygous non-necrotic mutants, were amplified using specific primer pairs (Supplementary Data 3) designed using IWGSC RefSeq v2.1[29] reference sequence with $B_{ATCH}P_{RIMER}3$ software[48]. PCR was performed in a Biometra T3000 Thermocycler (Applied Biosystems, New York, NY, USA) in 20 μL total volumes, consisting of 10 μL of PCR mixture (including *Taq* polymerase, dNTPs, and 10× PCR buffer with Mg^{2+}), 5 μL ddH_2O, 1 μL cDNA (50 ng μL^{-1}), and 2 μL of 10 μmol L^{-1} each of the forward and reverse primers. The thermal cycling profile is denaturation for 5 min at 95 °C, followed by 35 cycles of 30 s at 94 °C, 30 s at 59–62 °C, 2 min at 72 °C and a final extension for 10 min at 72 °C. The PCR products were sequenced by Sanger sequencing service (Beijing Tsingke Biotech Co., Ltd., Beijing, China) following the manufacturer's standard protocol. After the Sanger sequencing data is assembled, candidate genes for *Ne1* or *Ne2* genes obtained from the homozygous non-necrotic mutants and the wild type (M114 or NIL-*Ne1*) are subjected to multiple sequence alignment using the ClustalW (http://www.clustal.org/omega/) to confirm mutation sites.

Wheat transformation

To create *Ne1*-transgenic wheat plants, the coding sequence of *Ne1* was amplified from YBM and inserted into the pTA1037 vector using the EZ-HiFi Seamless Cloning Kit (GenStar, China). The resulting recombinant construct, *proUbi*::$Ne1^{YBM}$, containing the $Ne1^{YBM}$ gene regulated by the maize ubiquitin promoter[51], was transferred into the EHA105 strain and subsequently introduced into immature embryos of common wheat Fielder with the *ne1ne1ne2ne2* genotype via *Agrobacterium*-mediated transformation with the assistance of WeiMi Biotechnology Co., LTD, Jiangsu province, China. The $Ne1^{YBM}$ positive-transgenic plants was confirmed by the specific primer *OE-Ne1-L/R*, while the expression of *Ne1* was analyzed by primer *qNe1* (Supplementary Data 3). To conduct genetic complementation tests, line ZZ6903 (*ne1ne1Ne2Ne2*) was crossed with OE$Ne1^{YBM}$#1-#4 (*Ne1* homozygous transgenic lines, i.e., $Ne1^{YBM}Ne1^{YBM}$*ne1ne1ne2ne2*). In addition, a 13,118 bp genomic fragment of $Ne1^{M114}$, including the 2406 bp upstream of the start codon, the 8157 bp complete coding region and introns, and the 2555 bp downstream of the stop codon, was cloned into the vector pCAMBIA-1300. The recombinant construct was introduced into the homozygous *Ne2* overexpression transgenic line OE-T_1–1-1 (OE*Ne2*)[23] and Fielder × ZM F_1 hybrid plants, respectively, via *Agrobacterium* - mediated transformation. Specific PCR primer *Ne1HB-jc* was designed to validate the presence of *Ne1* in the transgenic plants. Primer *qNe1* was used to analyze the expression of *Ne1* in the transgenic plants. All transgenic plants for each transgenic event were planted in the greenhouse for phenotyping.

Quantitative real-time PCR analysis

Total RNA samples were extracted from leaves of NIL-*ne1* and NIL-*Ne1* using the TRIzol reagent (Invitrogen, USA), and expression analysis were performed according to the protocol established by Zhang et al. [52]. Five representative individual plants were selected, and equivalent quantities of leaf tissue were collected for RNA extraction. The first-strand cDNA from total RNA was synthesized using PrimeScript™ RT reagent Kit with gDNA Eraser (Perfect Real Time) (TaKaRa, Kyoto, Japan), and RT-qPCR was performed with SYBR green kit (TaKaRa, Kyoto, Japan) in a Roche 480 light cycler (Roche, Switzerland). The thermocycling conditions for the RT-qPCR included an initial denaturation of 3 min at 95 °C; 40 cycles of 30 s at 95 °C, 10 s at 58 °C, and 20 s at 68 °C, followed by a final extension of 5 min at 68 °C. The relative expression level of the gene was calculated using the $2^{-\Delta\Delta Ct}$ method[53]. RT-qPCR analysis was conducted with three biological replicates. Primers used to evaluate the transcript levels of *ABH.1* and pathogen-related marker genes, including *PR1*, *PR2*, *PR3*, *PR5*, and *LOX2* are listed in Supplementary Data 3. *TaActin* was used as an endogenous control (Supplementary Data 3). The student's *t* test was utilized to evaluate statistical significance.

Measurement of free SA and JA levels

The quantification of free SA and JA in NIL-*ne1* and NIL-*Ne1* plants was performed using liquid chromatography-tandem mass spectrometry (LC-MS/MS), as modified from the method described by Xiang et al.[54]. Fresh leaves were collected from 45-day-old NIL-*ne1* and NIL-*Ne1* plants and immediately frozen in liquid nitrogen. Approximately 50 mg of ground leaf tissue was weighed and transferred into a 1.5 mL tube. The samples were spiked with 10 μL of an internal standard mixture (100 ng/mL) and 1 mL of extraction solvent (methanol/water/formic acid, 15:4:1, v/v/v). The mixture was vortexed for 10 min and then centrifuged at 12,000 × *g* for 5 min at 4 °C. The supernatant was transferred to a new centrifuge tube and concentrated under vacuum.

The residue was reconstituted in 100 μL of 80% methanol/water solution, filtered through a 0.22 μm syringe filter, and transferred to an autosampler vial for LC-MS/MS analysis. The LC-MS/MS system consisted of an ExionLC™ AD ultra-performance liquid chromatography (UPLC) system coupled to a QTRAP® 6500 + tandem mass spectrometer (SCIEX, China). The chromatographic separation was achieved on a Waters ACQUITY UPLC HSS T3 C18 column (1.8 μm, 100 mm × 2.1 mm i.d.). The mobile phase consisted of (A) ultrapure water with 0.04% acetic acid and (B) acetonitrile with 0.04% acetic acid. The gradient elution program was as follows: 0 min, 95:5 (A/B, v/v); 1.0 min, 95:5 (A/B, v/v); 8.0 min, 5:95 (A/B, v/v); 9.0 min, 5:95 (A/B, v/v); 9.1 min, 95:5 (A/B, v/v); and 12.0 min, 95:5 (A/B, v/v). The flow rate was set at 0.35 mL/min, with a column temperature of 40 °C and an injection volume of 2 μL. The electrospray ionization (ESI) source was operated at 550 °C. The ionization voltage was set at + 5500 V in positive ion mode and − 4500 V in negative ion mode, with a curtain gas (CUR) pressure of 35 psi. The mass spectrometer was operated in multiple reaction monitoring (MRM) mode, and each ion pair was scanned with optimized declustering potential (DP) and collision energy (CE) values. Data acquisition and processing were performed using Analyst 1.6.3 and MultiQuant 3.0.3 software (SCIEX, China). The chromatographic peaks detected in the samples were integrated and corrected based on the retention time and peak shape information of the reference standards to ensure accurate qualitative and quantitative analysis. A total of six samples were analyzed, comprising three biological replicates each from NIL-*ne1* and NIL-*Ne1*.

Subcellular localization

A. tumefaciens-mediated transient gene expression in *N. benthamiana* assays was performed with minor modifications[32]. In short, the coding region of *Ne1* was cloned into the *pMDC43* vector and subsequently transformed into *Agrobacterium tumefaciens* GV3101. Then, the construct *pro35S::Ne1-GFP* was co-expressed with *PIP2-mCherry*, plasma membrane marker[32] in 4-week-old *N. benthamiana* leaves through *A. tumefaciens*-mediated infiltration. Following infiltration, the plants were incubated in a greenhouse at 25 °C for 48 h, and the fluorescence signals were assessed and captured using a laser confocal scanning microscope (Zeiss LSM780) in accordance with the manufacturer's guidelines.

Yeast signal sequence trap system

To assess the secretory capability of the Ne1 signal peptide (SP), we conducted a yeast secretion assay to measure yeast growth on sucrose or raffinose media[55]. Yeast transformation was carried out following the protocol of the Yeast maker™ Yeast Transformation System 2 (Clontech, USA). The invertase-deficient yeast strain (YTK12), negative (pSUC2-Mg87), and positive (pSUC2-Avr1b) control plasmids were generously provided by Professor Qianhua Shen from the Institute of Genetics and Developmental Biology, Chinese Academy of Sciences. The signal sequence of *Ne1* was predicted with the SignalP 4.1 server[56]. The predicted SP sequence of *Ne1* was amplified using specific primer *pSUC2-Ne1-SP-F/R* (Supplementary Data 3) and fused with a truncated *SUC2* gene that encodes an invertase lacking an SP via the EZ-HiFi Seamless Cloning Kit (GenStar, China). The resulting construct, *pSUC2-Ne1-SP*, was subsequently transformed into the yeast strain YTK12. After transformation, yeast cells were selected on yeast minimal tryptophan dropout plates (CMD-W) containing 2% sucrose, 2% agar, 0.67% yeast nitrogen base without amino acids, 0.1% glucose, and 0.075% tryptophan dropout supplement. Transformed colonies were transferred to fresh CMD-W medium and incubated at 30 °C for three days. For the invertase secretion assay, transformed yeast colonies were replica plated onto YPRAA plates (2% raffinose, 2% peptone, 2% agar, 1% yeast extract, and 2 μg/mL antimycin A). After three days of incubation at 30 °C, the plates were evaluated for growth and imaged. In addition, 2, 3, 5-triphenyltetrazolium chloride (TTC) dye conversion to the insoluble red-colored triphenylformazan was used to verify invertase secretion.

Structural and allelic variation analysis for *Ne1*

For the structural and allelic variation analysis of *Ne1*, 540 hexaploid wheat[33–35] (Supplementary Data 5), and 157 tetraploid wheat genome re-sequencing data[35–37] (Supplementary Data 6) were analyzed. Reads from these samples were mapped to IWGSC RefSeq v2.1[29] with bwa software (https://sourceforge.net/projects/bio-bwa/files/) with default parameter settings. The ensuing coverage depth for every 5 kilobase (kb) window was ascertained with mosdepth software (https://github.com/brentp/mosdepth), incorporating parameter settings (-n –fast-mode –by 5000 -F 1796 -Q 40). The coverage depth for every 5 kb window was later normalized based on each sample's total coverage depth. Furthermore, 157 tetraploid wheat genome re-sequencing data[35–37] and nine Sitopsis genome data[39,40] were utilized to conduct an origin analysis of *Ne1*.

Copy number variation validation of *Ne1*

In this study, we employed RT-qPCR technology to statistically analyze the relative copy number of *Ne1* (Supplementary Data 3 and 8). Building upon previous research, we identified that *Ne2* lacks homologs in the common wheat genome, existing as a single copy[22], making it an endogenous control gene. We designed specific markers, *qCNV-Ne1-F/R* and *qCNV-Ne2-F/R*, targeting the unique sequences of *Ne1* and *Ne2*, respectively. Genomic DNA was extracted from plant leaves using the cetyltrimethylammonium bromide (CTAB) method[47]. The relative copy number of *Ne1* was determined following the experimental procedures and data analysis methods described above for gene expression level detection, with the modification that genomic DNA was utilized in place of cDNA in the reaction mixture.

Distribution of *Ne1*

We designed and validated a dominant marker, *Ne1-Select2128* (Supplementary Data 3), targeting the specific sequence of *Ne1*. This marker can effectively detect the presence or absence of *Ne1* alleles in both tetraploid and hexaploid wheat accessions. For *Ne1-Select2128*, each PCR reaction (10 μL) consisted of 5 μL 2 × Taq PCR Starmix (GenStar, China), 0.5 μL of 10 μM sense and antisense primers, 2 μL DNA template (approximately 50-90 ng), and 2 μL ddH_2O. The PCR thermocycling involved an initial denaturation at 95 °C for 5 min, followed by 8 cycles of 94 °C for 30 s, 64 °C with a 0.7 °C reduction per cycle for 30 s, 72 °C for 30 s; and 25 cycles of 30 s at 94 °C, 30 s at 57 °C, 30 s at 72 °C, culminating with a final extension of 2 min at 72 °C. The PCR products were then assessed and visualized by electrophoresis on 1% agarose gels. Materials carrying *Ne1* can be amplified using *Ne1-Select2128*, producing a distinct 1,110 bp band. A functional marker *Ne2-Select91* for the detection of *Ne2* was also developed[22]. In addition, to visualize the geographic distribution of the *Ne1* allele, we generated proportional symbol maps using ArcMap 10.8.1[57]. The maps were constructed using both national and global base maps, with underlying data sourced from Shapefile files[57].

Statistics and reproducibility

In the study, we conducted most experiments with three biological replicates, except the RNA-seq data from 305 common wheat samples used to quantify *ABH.1* expression for the four CNV groups represents a single biological replicate. Sample sizes were chosen based on our prior experience and the standard practices in the field. No statistical method was used to predetermine the sample size. All experiments were designed and conducted with randomization in the selection of samples to minimize potential biases. The investigators were blinded to the allocation during experiments and outcome assessment to ensure unbiased data collection and analysis. No data were excluded from the analyses. To further ensure the reproducibility of our

experiments, we followed standardized protocols and used the same reagents and equipment across all replicates. Statistical analyses were conducted (two-sided Student's *t* test), and charts were created using GraphPad Prism 8 (GraphPad Software). The sequence alignment charts were produced using DNAMAN version 8.

Primers
All the primers used in this study are listed in Supplementary Data 3.

Reporting summary
Further information on research design is available in the Nature Portfolio Reporting Summary linked to this article.

Data availability
The sequencing data generated in this study have been deposited in the Genome Sequence Archive in the National Genomics Data Center (NGDC), China National Center for Bioinformation/Beijing Institute of Genomics, Chinese Academy of Sciences database under accession code CRA005878. The *Ne2* and multiple *Ne1* alleles sequence data generated in this study have been deposited in the GenBank database under accession code: *Ne2* (MW756036), *Ne1-MI14* (PP781974), *Ne1-CS* (PP760338), *Ne1-YM14* (PP760339), *Ne1-YBM* (PP760340), *Ne1-PI182704* (PP760341), *Ne1-Mania* (PP760342). Source data are provided in this paper.

References

1. Bomblies, K. & Weigel, D. Hybrid necrosis: autoimmunity as a potential gene-flow barrier in plant species. *Nat. Rev. Genet.* **8**, 382–393 (2007).
2. Li, L. & Weigel, D. One hundred years of hybrid necrosis: hybrid autoimmunity as a window into the mechanisms and evolution of plant-pathogen interactions. *Annu. Rev. Phytopathol.* **59**, 213–237 (2021).
3. Chae, E. et al. Species-wide genetic incompatibility analysis identifies immune genes as hot spots of deleterious epistasis. *Cell* **159**, 1341–1351 (2014).
4. Bomblies, K. et al. Autoimmune response as a mechanism for a Dobzhansky-Muller-type incompatibility syndrome in plants. *PLoS Biol.* **5**, e236 (2007).
5. Sicard, A. et al. Divergent sorting of a balanced ancestral polymorphism underlies the establishment of gene-flow barriers in *Capsella*. *Nat. Commun.* **6**, 7960 (2015).
6. Hermsen, J. G. T. The genetic basis of hybrid necrosis in wheat. *Genetica* **33**, 245–287 (1963).
7. Ren, Z. L. & Lelley, T. Genetics of hybrid necrosis in Rye. *Plant Breed.* **100**, 173–180 (1988).
8. Jeuken, M. J. et al. *Rin4* causes hybrid necrosis and race-specific resistance in an interspecific lettuce hybrid. *Plant Cell* **21**, 3368–3378 (2009).
9. Chen, C. et al. A two-locus interaction causes interspecific hybrid weakness in rice. *Nat. Commun.* **5**, 3357 (2014).
10. Deng, J., Fang, L., Zhu, X., Zhou, B. & Zhang, T. A CC-NBS-LRR gene induces hybrid lethality in cotton. *J. Exp. Bot.* **70**, 5145–5156 (2019).
11. Dobzhansky T. Genetics and the origin of species. (New York: Columbia Univeristy Press, 1937).
12. Muller, H. J. Isolating mechanisms, evolution, and temperature. *Biol. Symp.* **6**, 71–125 (1942).
13. Orr, H. A. Dobzhansky, Bateson, and the genetics of speciation. *Genetics* **144**, 1331–1335 (1996).
14. Li, X. et al. Large-scale gene expression alterations introduced by structural variation drive morphotype diversification in *Brassica oleracea*. *Nat. Genet.* **56**, 517–529 (2024).
15. Qiao, X. et al. Gene duplication and evolution in recurring polyploidization–diploidization cycles in plants. *Genome Biol.* **20**, 38 (2019).
16. Wang, Y. et al. Copy number variation at the *GL7* locus contributes to grain size diversity in rice. *Nat. Genet.* **47**, 944–948 (2015).
17. Lee, T. G., Diers, B. W. & Hudson, M. E. An efficient method for measuring copy number variation applied to improvement of nematode resistance in soybean. *Plant J.* **88**, 143–153 (2016).
18. Shen, R. et al. Genomic structural variation-mediated allelic suppression causes hybrid male sterility in rice. *Nat. Commun.* **8**, 1310 (2017).
19. Sax, K. Sterility in wheat hybrids. I. sterility relationships and endosperm development. *Genetics* **6**, 399–416 (1921).
20. Mizuno, N., Shitsukawa, N., Hosogi, N., Park, P. & Takumi, S. Autoimmune response and repression of mitotic cell division occur in inter-specific crosses between tetraploid wheat and *Aegilops tauschii* Coss. that show low temperature-induced hybrid necrosis. *Plant J.* **68**, 114–128 (2011).
21. Chu, C. G., Faris, J. D., Friesen, T. L. & Xu, S. S. Molecular mapping of hybrid necrosis genes *Ne1* and *Ne2* in hexaploid wheat using microsatellite markers. *Theor. Appl. Genet.* **112**, 1374–1381 (2006).
22. Si, Y. et al. *Ne2*, a typical CC-NBS-LRR-type gene, is responsible for hybrid necrosis in wheat. *New Phytol.* **232**, 279–289 (2021).
23. Yan, X. et al. High-temperature wheat leaf rust resistance gene *Lr13* exhibits pleiotropic effects on hybrid necrosis. *Mol. Plant* **14**, 1029–1032 (2021).
24. Hewitt, T. et al. Wheat leaf rust resistance gene *Lr13* is a specific *Ne2* allele for hybrid necrosis. *Mol. Plant* **14**, 1025–1028 (2021).
25. Athiyannan, N. et al. Long-read genome sequencing of bread wheat facilitates disease resistance gene cloning. *Nat. Genet.* **54**, 227–231 (2022).
26. Si, Y. et al. Fine mapping of hybrid necrosis gene *Ne1* in common wheat (*Triticum aestivum* L.). *Theor. Appl. Genet.* **134**, 2603–2611 (2021b).
27. Li, N., Tan, Q., Ding, J., Pan, X. & Ma, Z. Fine mapping of *Ne1*, the hybrid necrosis gene complementary to *Ne2* in common wheat (*Triticum aestivum* L.). *Theor. Appl. Genet.* **134**, 2813–2821 (2021).
28. Zhang, M. et al. Fine mapping and distribution analysis of hybrid necrosis genes *Ne1* and *Ne2* in wheat in China. *Theor. Appl. Genet.* **135**, 1177–1189 (2022).
29. Zhu, T. et al. Optical maps refine the bread wheat *Triticum aestivum* cv. Chinese Spring genome assembly. *Plant J.* **107**, 303–314 (2021).
30. Jia, A. et al. TIR-catalyzed ADP-ribosylation reactions produce signaling molecules for plant immunity. *Science* **377**, eabq8180 (2022).
31. Pruitt, R. N. et al. The EDS1-PAD4-ADR1 node mediates *Arabidopsis* pattern-triggered immunity. *Nature* **598**, 495–499 (2021).
32. Lee, H. K. et al. Drought stress-induced Rma1H1, a RING membrane-anchor E3 ubiquitin ligase homolog, regulates aquaporin levels via ubiquitination in transgenic *Arabidopsis* plants. *Plant Cell* **21**, 622–641 (2009).
33. Niu, J. et al. Whole-genome sequencing of diverse wheat accessions uncovers genetic changes during modern breeding in China and the United States. *Plant Cell* **35**, 4199–4216 (2023).
34. Hao, C. et al. Resequencing of 145 landmark cultivars reveals asymmetric sub-genome selection and strong founder genotype effects on wheat breeding in China. *Mol. Plant* **13**, 1733–1751 (2020).
35. Zhou, Y. et al. *Triticum* population sequencing provides insights into wheat adaptation. *Nat. Genet.* **52**, 1412–1422 (2020).
36. Wang, H. et al. Sympatric speciation of wild emmer wheat driven by ecology and chromosomal rearrangements. *Proc. Natl. Acad. Sci. USA* **117**, 5955–5963 (2020).
37. Wang, Z. et al. Dispersed emergence and protracted domestication of polyploid wheat uncovered by mosaic ancestral haploblock inference. *Nat. Commun.* **13**, 3891 (2022).
38. Vikas, V. K. et al. Hybrid necrosis in wheat: evolutionary significance or potential barrier for gene flow? *Euphytica* **194**, 261–275 (2013).

39. Li, L. F. et al. Genome sequences of five Sitopsis species of *Aegilops* and the origin of polyploid wheat B subgenome. *Mol. Plant* **15**, 488–503 (2022).
40. Yang, Y. et al. Genome sequencing of Sitopsis species provides insights into their contribution to the B subgenome of bread wheat. *Plant Commun.* **4**, 100567 (2023).
41. Anonymous (1973) CIMMYT annual report on maize and wheat improvement 1972.
42. Anonymous (1976) CIMMYT annual report on maize and wheat improvement 1974.
43. Fitzgerald, H. A., Chern, M. S., Navarre, R. & Ronald, P. C. Overexpression of (*At*)*NPR1* in rice leads to a BTH- and environment-induced lesion-mimic/cell death phenotype. *Mol. Plant Microbe* . **17**, 140–151 (2007).
44. Xie, J. et al. A rare single nucleotide variant in *Pm5e* confers powdery mildew resistance in common wheat. *New Phytol* **228**, 1011–1026 (2020).
45. Dobin, A. et al. STAR: ultrafast universal RNA-seq aligner. *Bioinformatics* **29**, 15–21 (2013).
46. McKenna, A. et al. The Genome Analysis Toolkit: a MapReduce framework for analyzing next-generation DNA sequencing data. *Genome Res.* **20**, 1297–1303 (2010).
47. Allen, G. C., Flores-Vergara, M. A., Krasynanski, S., Kumar, S. & Thompson, W. F. A modified protocol for rapid DNA isolation from plant tissues using cetyltrimethylammonium bromide. *Nat. Protoc.* **1**, 2320–2325 (2006).
48. You, F. M. et al. BatchPrimer3: a high throughput web application for PCR and sequencing primer design. *BMC Bioinform.* **9**, 253 (2008).
49. Lincoln, S. E., Daly, M. J. & Lander, E. S. Constructing linkage maps with MAPMAKER/Exp Version 3.0. A tutorial reference manual, 3rd edn. (Whitehead Institute for Medical Res., Cambridge, MA 1993).
50. Saintenac, C. et al. Identification of wheat gene *Sr35* that confers resistance to Ug99 stem rust race group. *Science* **341**, 783–786 (2013).
51. Cornejo, M. J., Luth, D., Blankenship, K. M., Anderson, O. D. & Blechl, A. E. Activity of a maize ubiquitin promoter in transgenic rice. *Plant Mol. Biol.* **23**, 567–581 (1993).
52. Zhang, Y. et al. Mediator subunit 16 functions in the regulation of iron uptake gene expression in *Arabidopsis*. *New Phytol.* **203**, 770–783 (2014).
53. Livak, K. J. & Schmittgen, T. D. Analysis of relative gene expression data using real-time quantitative PCR and the $2^{-\Delta\Delta CT}$ method. *Methods* **25**, 402–408 (2001).
54. Xiang, Y. A jacalin-related lectin-like gene in wheat is a component of the plant defence system. *J. Exp. Bot.* **62**, 5471–5483 (2011).
55. Oh, S. K. et al. In planta expression screens of RXLR effectors reveal diverse phenotypes, including activation of the disease resistance protein Rpi-blb2. *Plant Cell* **21**, 2928–2947 (2009).
56. Nielsen, H. Predicting secretory proteins with SignalP. *Methods Mol. Biol.* **1611**, 59–73 (2017).
57. ESRI. ArcGIS Desktop: Release 10.8.1. Environmental Systems Research Institute, Redlands. (2020).

Acknowledgements

This work was supported by the STI 2030–Major Projects (2023ZD04070 to M.M.L.), the Strategic Priority Research Program of the Chinese Academy of Sciences (XDA24010204 to H.-Q.L.), the National Natural Science Foundation of China (31991211 to H.-Q.L.; 32101735 to M.M.L.; 32302364 to X.C.Y.; U21A20224 to Z.Y.L.), the National Key Research and Development Program of China (2023YFF1000600 to L.L.D. and 2023YFD1200402 to Z.Y.L.), the Major Project of Agricultural Biological Breeding (2023ZD0402501 to H.Z.Z.), the Major Basic Research Program of Shandong Natural Science Foundation (ZR2019ZD15 to H.-Q.L.). This project was also supported by grants from the Hainan Seed Industry Laboratory (B21HJ0111 to Z.Y.L.), China Postdoctoral Science Foundation (2022M710163 to Y.Q.S.), Key Research and Development Program of Hebei (22326305D to C.G.Y.) and Yazhouwan National Laboratory project (2310JM01 to S.W.M.).

Author contributions

H.-Q.L., Z.L., M.L., and L.L.D. conceived and designed the study. Y.S., H.Z., S.Z., J.N., S.T., X.C., K.Z., Q.L., Z.Z., T.D., P.L., M.G., Y.C., and Q.W. carried out the experiments, conducted fieldwork and analyzed data. S.M., J.X., G.G., and L.L.D. performed bioinformatic analysis. Z.F.L., X.Y., C.Y., Y.L., and H.W. provided germplasm, scientific support, and advice. H.-Q.L., Z.L., M.L., and Y.S. wrote the manuscript. All authors contributed to the article and approved the submitted version.

Competing interests

The authors declare no competing interests.

Additional information

Supplementary information The online version contains supplementary material available at https://doi.org/10.1038/s41467-025-57750-5.

Correspondence and requests for materials should be addressed to Zhiyong Liu, Lingli Dong, Hong-Qing Ling or Miaomiao Li.

Peer review information *Nature Communications* thanks André Laroche and the other anonymous reviewers for their contribution to the peer review of this work. A peer review file is available.

Reprints and permissions information is available at http://www.nature.com/reprints

Publisher's note Springer Nature remains neutral with regard to jurisdictional claims in published maps and institutional affiliations.

Open Access This article is licensed under a Creative Commons Attribution-NonCommercial-NoDerivatives 4.0 International License, which permits any non-commercial use, sharing, distribution and reproduction in any medium or format, as long as you give appropriate credit to the original author(s) and the source, provide a link to the Creative Commons licence, and indicate if you modified the licensed material. You do not have permission under this licence to share adapted material derived from this article or parts of it. The images or other third party material in this article are included in the article's Creative Commons licence, unless indicated otherwise in a credit line to the material. If material is not included in the article's Creative Commons licence and your intended use is not permitted by statutory regulation or exceeds the permitted use, you will need to obtain permission directly from the copyright holder. To view a copy of this licence, visit http://creativecommons.org/licenses/by-nc-nd/4.0/.

© The Author(s) 2025